Self-Assembled Pt/Mesoporous Silica–Carbon Electrocatalysts for Elevated-Temperature Polymer Electrolyte Membrane Fuel Cells

ARTICLE *in* THE JOURNAL OF PHYSICAL CHEMISTRY C · NOVEMBER 2008

Impact Factor: 4.77 · DOI: 10.1021/jp8066662

2 AUTHORS:

Haolin Tang
Wuhan University of Technology
101 PUBLICATIONS **1,843** CITATIONS

SEE PROFILE

San Ping Jiang
Curtin University
345 PUBLICATIONS **11,469** CITATIONS

SEE PROFILE

Article

Self-Assembled Pt/Mesoporous Silica#Carbon Electrocatalysts for Elevated-Temperature Polymer Electrolyte Membrane Fuel Cells

Haolin Tang, and San Ping Jiang

J. Phys. Chem. C, **2008**, 112 (49), 19748-19755• DOI: 10.1021/jp8066662 • Publication Date (Web): 14 November 2008

Self-Assembled Pt/Mesoporous Silica−Carbon Electrocatalysts for Elevated-Temperature Polymer Electrolyte Membrane Fuel Cells

Haolin Tang[†,‡] **and San Ping Jiang***[,†]

School of Mechanical and Aerospace Engineering, Nanyang Technological University, 50 Nanyang Avenue, Singapore 639798, and State Key Laboratory of Advanced Technology for Materials Synthesis and Processing, Wuhan University of Technology, Wuhan 430070, PR China

Received: July 28, 2008; Revised Manuscript Received: October 10, 2008

Mesoporous carbon and silica−carbon have been synthesized through a hydrogen-bonding-assisted self-assembly route as Pt electrocatalyst supports for polymer electrolyte membrane fuel cells (PEMFCs). Solid-state ^{1}H NMR analysis indicates the condensation of water inside the capillaries of the mesoporous structure, and the water condensation is increased by the incorporation of hydrophilic silica in the mesoporous carbon. The pore diameters of the Pt/meso-carbon and Pt/meso-SiO_2−carbon electrocatalysts were 4.5 and 5.2 nm, respectively. The use of meso-carbon and meso-SiO_2−carbon supports to replace conventional XC-72 carbon black significantly improves the fuel cell performance when operating at an elevated temperature of 100 °C and a reduced relative humidity of 30%. The cell assembled with the Pt/meso-SiO_2−carbon electrocatalysts produced a maximum power density of 456 mW cm^{-2} at 100 °C and 30% RH, higher than 417 and 345 mW cm^{-2} for the cells with Pt/meso-carbon and Pt/XC-72 carbon electrocatalysts, respectively.

1. Introduction

Proton-exchange membrane fuel cells (PEMFCs) have attracted much attention as clean energy technologies because of their high power density and high efficiency with low greenhouse gas emission levels for various applications such as electric vehicles, portable electronics, and residential power generation.[1] However, it is realized that it is necessary and important to increase the operating temperatures of PEMFCs to accelerate the oxygen reduction reaction (ORR) kinetics and reduce catalyst poisoning.[2,3] The overpotential at the cathode (ORR electrode) accounts for the major voltage loss of PEMFC and is considered to be one of the determining processes that limit the fuel cell performance. The sluggish ORR kinetics can be significantly improved with the increase in operating temperature.[4] The CO tolerance of Pt-based electrocatalysts will also be enhanced significantly for cells operated at elevated temperatures.

The major challenge in the increase of the operating temperature is to enhance the thermal stability and water retention properties of membrane−electrode assemblies (MEAs).[5] Though significant efforts have been made to modify the polymer electrolyte membrane for application at elevated temperatures or for low-humidity fuel cells,[3,6] the increase in fuel cell operating temperature is still impeded by the low thermal stability and low water retention ability of the electrocatalyst layer in MEA. The water retention of conventional electrocatalyst layers is limited by the low content of the hydrophilic phase such as the Nafion electrolyte in the catalyst layer. Rapid dehydration at elevated temperatures further deteriorates the water retention ability of the catalyst electrode, resulting in further reduction in the proton conductivity in the catalyst electrode and thus decreasing the cell performance. Thus, the challenge is to improve the proton conductance and the water retention properties of the electrocatalyst layer for the PEMFCs operated at elevated temperatures and low humidity.

To increase the operating temperature of the electrocatalyst layer in MEA, one approach is to incorporate hygroscopic metal oxide particles such as SiO_2 or zirconium phosphate into the catalyst supports and the hydrophilic domain to enhance the water retention properties (i.e., self-humidifying) in the catalyst layer.[7,8] The results show that the incorporation of hydrophilic particles in the anode catalyst layer increases the hydration of the catalyst layer at low RH values and thus improves the proton conduction. However, because the additives are nonproton and nonelectron conductive, the addition of excess hydrophilic particles such as silica to the catalyst layer would inhibit proton or electron conduction, resulting in a low cell performance.[8] Another approach is to develop a functionally graded gas diffusion layer (GDL) that is in intimate contact with the catalyst layer and hence could provide moisture to maintain the humidity of the catalyst electrode.[9] However, it is not an easy task to fabricate an effective functionally graded gas diffusion layer with a reproducible porosity distribution.

It is known that capillary condensation occurs in narrow hydrophilic channels or pores and that the saturation vapor pressure decreases with the decrease in the size of the capillaries.[10,11] Thus, replacing the commonly used carbon supports with one with nanosized hydrophilic channels, such as mesoporous carbon, is an effective way to maintain the humidity in the electrocatalyst layer operated under elevated-temperature or low-humidity conditions. In fact, applications of mesoporous carbon as electrocatalyst supports have received more and more attention recently.[12] An early report found that mesoporous carbon with highly dispersed Pt nanoparticles improves the electrocatalytic activity for the oxygen reduction reaction.[13,14] The superiority of mesoporous carbon as electrocatalyst supports is attributed to the high accessible surface area provided by the ordered mesopores.[15] The Pt electrocatalyst supported on mesoporous carbon almost doubled the specific

* Corresponding author. Tel: +65-6790 5010. E-mail address: mspjiang@ntu.edu.sg.
† Nanyang Technological University.
‡ Wuhan University of Technology.

10.1021/jp8066662 CCC: $40.75
Published on Web 11/14/2008

mass activities as compared to that supported on conventional XC-72 high surface area carbon,[16] and the nanochannel architecture of the mesoporous supports also has the potential to enhance the active surface area and to improve the transport of reactant species, hence enhancing the activity of the catalyst.[17]

In the present work, we synthesized and developed a high-performance Pt electrocatalyst supported on a new mesoporous silica−carbon. The hydrophilic silica was anchored into the mesoporous carbon through a self-assembly route between the silica and the carbon source. Thus, the hydrophilic silica incorporated into the mesoporous carbon increases the water retention property of the supports, enhancing the self-humidifying ability of the Pt electrocatalysts in the electrocatalyst layer during the fuel cell operation at elevated temperature and low humidity.

2. Experimental Section

2.1. Synthesis of Mesoporous Carbon and Mesoporous Silica−Carbon Supports. The ordered mesoporous carbon supports were synthesized on the basis of a report by Liang and Dai.[18] To prepare the pure mesoporous carbon, 2.5 g of phloroglucinol (Sigma-Aldrich) and 2.5 g of P123 (nonionic triblock copolymer $EO_{20}PO_{70}EO_{20}$, Sigma-Aldrich) were dissolved in 19 g of an ethanol/water solution (10:9 weight ratio). After the chemicals were dissolved under magnetic stirring at room temperature, 0.3 g of HCl (37 wt %, Sigma-Aldrich) was added to the solution. The solution was stirred at room temperature for 0.5 h until a light-pink color appeared. Subsequently, 2.6 g of formaldehyde (Sigma-Aldrich) dissolved in an ethanol/water solution was added to the above solution. The solution turned cloudy after ~30 min, and phase separation occurred after ~1 h. The lower portion of the solution of mainly phenol formaldehyde was applied to substrates by spin coating at 2000 rpm. The film was cured at room temperature for 4 h and then at 100 °C overnight. The resulting complex was carbonized in a tubular furnace under a nitrogen atmosphere with heating ramps of 1 °C/min from 100 to 400 °C and 5 °C/min from 400 to 850 °C and was kept at 850 °C for 2 h. The mesoporous carbon was finally activated in a CO_2 atmosphere at 200 °C for 4 h and denoted as meso-carbon.

The above process was modified to introduce silica molecules into the mesoporous carbon nanostructure. To prepare the silica-incorporated mesoporous carbon, 2.5 g of phloroglucinol and 2.5 g of P123 were dissolved in 20 g of deionized water. After the chemicals were dissolved under magnetic stirring at room temperature, 0.3 g of 37% HCl was added to the solution, which was stirred at room temperature for another 0.5 h until a light-pink color appeared. Subsequently, 2.6 g of formaldehyde and 0.7 g of tetraethoxysilane (TEOS, 99.9%, Sigma-Aldrich) dissolved in 18 g of ethanol was added. The solution turned cloudy after ~30 min, and phase separation occurred after ~1 h. Similar to the above process, silica-incorporated mesoporous carbon was finally activated in a CO_2 atmosphere at 200 °C for 4 h. The SiO_2 content was 5 wt % in mesoporous carbon, and the product was denoted as meso-SiO_2−carbon.

2.2. Pt Electrocatalyst Preparation. The Pt electrocatalysts supported on meso-carbon, meso-SiO_2−carbon, and carbon black (XC-72, Cabot Corp., $S_{BET} \approx 240$ m^2 /g) were prepared by a pulse-microwave-assisted polyol route.[19] Chloroplatinic acid with a Pt content of 0.15 g was well mixed with ethylene glycol (EG, 100 mL) in a beaker by ultrasonic treatment for 30 min, and then 0.35 g of a carbon support (meso-carbon, meso-SiO_2−carbon, or carbon black) was added to the mixture. The pH value of the mixed suspension was adjusted to 10 by the dropwise addition of 1.0 mol/L NaOH/EG solution. After being dispersed by high-speed stirring and ultrasonication for 30 min, the Pt ions in the suspension were reduced to Pt^0 by three intermittent microwave heating cycles with pulses every 5 s. After the reduction, the pH value of the suspension was adjusted to 2 by HCl to promote the adsorption of the Pt nanoparticles onto the carbon support. The resulting electrocatalyst powders were filtered, washed, and dried at 80 °C for 10 h in a vacuum oven. The as-prepared Pt electrocatalysts supported on meso-carbon, meso-SiO_2−carbon, and XC-72 were denoted as Pt/meso-carbon, Pt/meso-SiO_2−carbon, and Pt/C, respectively.

2.3. Structure Characterization of Supports and Catalysts. Small-angle X-ray diffraction (SAXRD) patterns of the samples were recorded on a Rigaku D/MAX-RB diffractometer at 40 kV, 50 mA with Cu Kα radiation and a counter rate of 2°/min from $2\theta = 0.7-10°$. For transmission electron microscopy (TEM) experiments, samples were first suspended in acetone (99.9 vol %) by ultrasonication, followed by deposition of the suspension on a lacey carbon grid. TEM images were obtained using an electron microscopy (JEOL JEM-2100F). Nitrogen adsorption−desorption data were measured with a Quantachrome Autosorb-1 analyzer at 77 K. The surface area was calculated by the Brunauer−Emmett−Teller (BET) method. The pore-size distribution was derived from the isothermal adsorption curves using the Barrett−Joyner−Halenda (BJH) method. Before the measurements, samples were degassed for 12 h at 550 K. The solid-state NMR spectra of samples were carried out on a Varian InfinityPlus-400 spectrometer equipped with a 2.5 mm double-resonance magic-angle spinning probe. The probe pulses were 90 Ω with a duration of 2 μs. The relative mean error in the ^1H NMR signal intensity was ±10%.

2.4. Electrochemical Measurement and Fuel Cell Performance. Electrochemical measurements of the Pt electrocatalyst were performed on a galvanostat/potentiostat (Autolab, PGSTAT30) with a three-electrode cell at room temperature. A saturated calomel electrode (SCE) and a platinum foil were used as the reference and counter electrodes, respectively. A glass carbon (GC) working electrode was polished using 0.3 and 0.05 μm alumina slurries, followed by washing with water and acetone. Five milligrams of catalyst was dispersed ultrasonically in 1 mL of Nafion solution (0.5 wt %) to obtain a homogeneous ink. A 4.0 μL quantity of the ink was pipetted onto the GC electrode surface. The coating was then dried at room temperature in air. Cyclic voltammograms were collected in N_2-saturated 0.5 M H_2SO_4 between −0.23 and 1.0 V with a scan rate of 10 mV/s. The GC working electrodes were electrochemically cleaned by continuous cycling at 50 mV/s until a stable response was obtained before the measurement curves were recorded.

MEAs of the single cells were prepared as follows:[20] First, catalyst inks were prepared by mixing the Pt electrocatalyst, 5 wt % Nafion solution (DuPont D520), and isopropyl alcohol with a weight ratio of 1:6:10 under vigorous stirring. Then the catalyst slurry was screen printed onto the GDL (TGP-060, Toray Inc.) to form the electrocatalyst layer. Pt loading was 0.2 and 0.4 mg/cm^2 for the anode and cathode, respectively. The catalyst layer was dried at 60 °C for 10 min and at 90 °C in a N_2 atmosphere for 3 min. The Nafion 112 membrane (50 μm) and electrocatalyst layers were bonded together by hot pressing under 10 MPa at 125 °C for 90 s. Single fuel cells were assembled with the as-prepared MEAs and graphite flow field plates under a pressure of 10 MPa. The active area of the cell was 2×2 cm^2. H_2 and air were used as the fuel and oxidant without back pressure. The flow rates of H_2 and air were 300

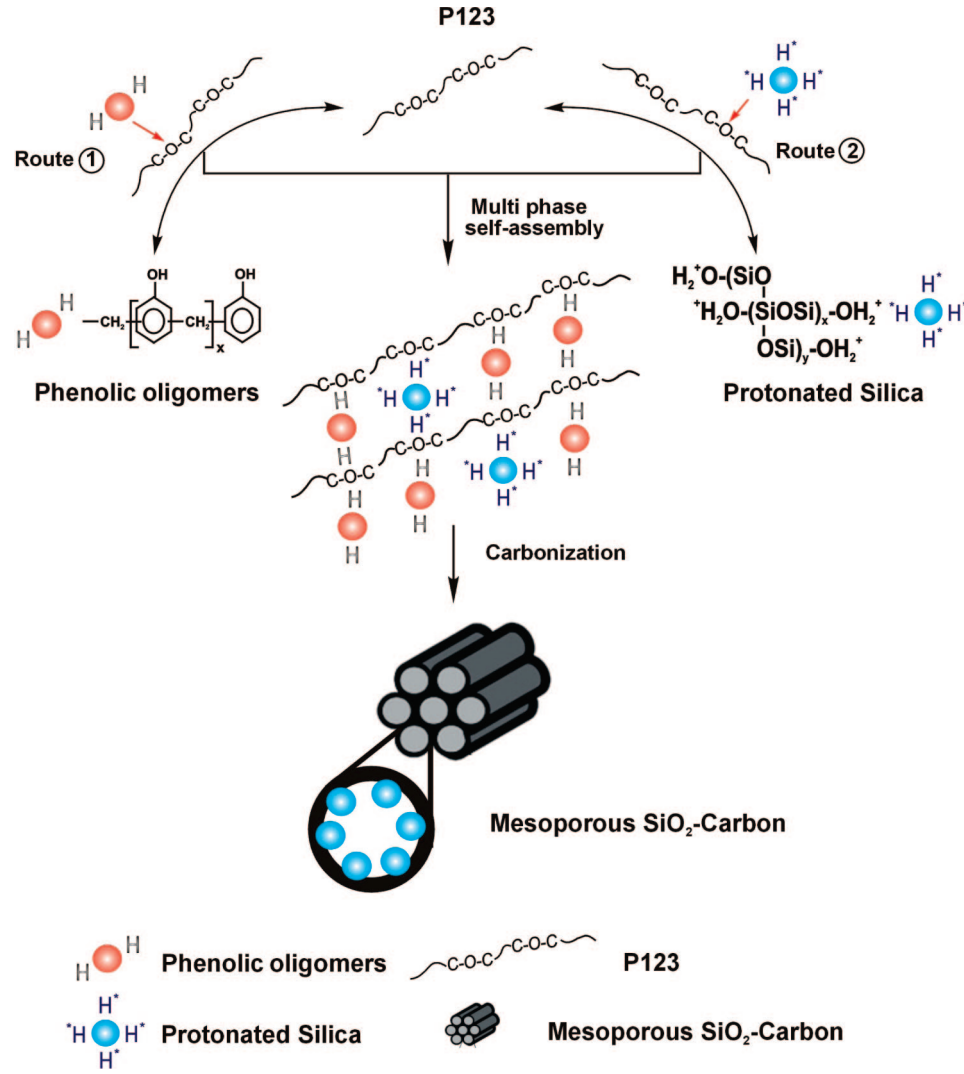

Figure 1. Schematic diagram of the formation of SiO_2-doped mesoporous carbon nanostructures.

and 2000 sccm, respectively. Cell performances were recorded by a Solartron 1260. Prior to the measurement, cells were activated by polarization at a constant current until stable performance was obtained.

Electrochemical impedance spectroscopy (EIS) of single cells was investigated using an Autolab Electrochemical station (PGSTAT30, The Netherlands) in potentiostatic mode at a cell voltage close to OCV (i.e., 0.85−0.90 V) with an amplitude of 5 mV over a frequency range of 10 mHz to 10 KHz. Because of the much faster reaction kinetics of the H_2 oxidation reaction on the Pt electrocatalysts as compared to that of the O_2 reduction reaction, the cell impedance would be mainly dominated by the cathodic impedance for the O_2 reduction reaction. The cell membrane resistance, R_m, was measured from the high-frequency intercept, and the polarization (or charge-transfer) resistance, R_{ct}, was obtained from the differences between the low- and high-frequency intercepts on the impedance curves.

3. Results and Discussion

3.1. Characteristics of Pt Electrocatalysts Supported on a meso-SiO_2−Carbon Nanostructure. The feasibility of preparing ordered mesoporous carbon through hydrogen-bonding-assisted self-assembly between hydroxyl (−OH) groups on hydrocarbon polymer and PEO-containing block copolymers has been demonstrated recently.[18,21] In this method, formaldehyde and phloroglucinol are polymerized to form phenolic oligomers in the presence of HCl catalyst, and many of the −OH groups would remain in the phenolic oligomers because of superfluous phloroglucinol in a stoichiometric ratio. Thus, the phenolic oligomers with high hydroxy density will be self-assembled onto the P123 surfactant between hydroxyl (−OH) groups on hydrocarbon polymer and PEO domains of PEO-PPO-PEO triblock copolymers. Then the ordered P123/carbohydrates nanocomposites are formed with the phase separation of structure-directing surfactant P123. The phenolic oligomers are further polymerized to form dense networks by curing at 100 °C. After treatment at high temperature in N_2, the hydrocarbon matrixes were carbonized, forming the mesoporous carbon.

Figure 1 schematically illustrates the formation of meso-SiO_2−carbon based on a modified hydrogen-bonding-assisted self-assembly process. Besides the self-assembly between the phenolic oligomers and PEO-containing P123 block polymer (route 1 in Figure 1), the in-situ-formed silica molecules at pH <2 also can be self-assembled to PEO chains of P123 block polymer because of the protonated surface of the SiO_2.[22] The protonation of SiO_2 nanostructures likely resulted from the acidic hydrolysis reaction of the TEOS and was promoted by the high acidity of the solution. For amorphous silica, two types of surface groups (singly and doubly Si-coordinated) are present, and they differ in their affinity for the adsorption of a proton.[23]

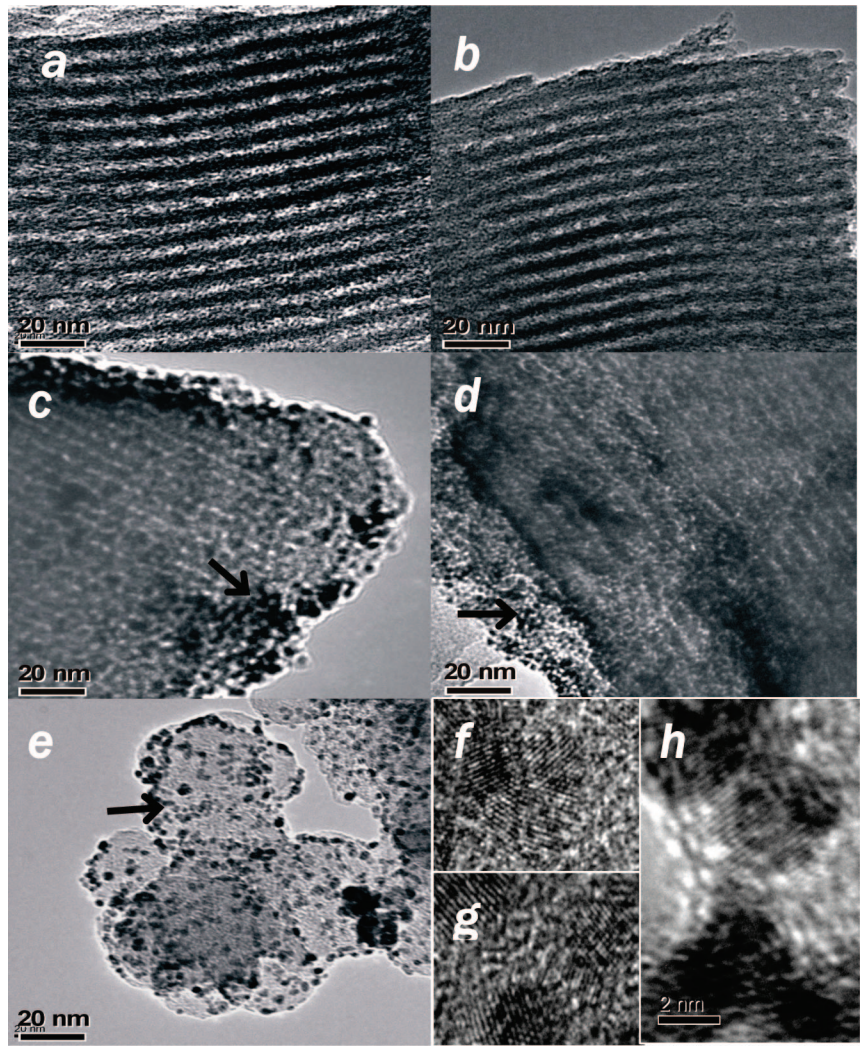

Figure 2. High-resolution TEM images of (a) meso-carbon, (b) meso-SiO_2−carbon, (c) Pt/meso-carbon, (d) Pt/meso-SiO_2−carbon, (e) Pt/C, (f) Pt nanoparticles of Pt/meso-carbon, (g) Pt nanoparticles of Pt/meso-SiO_2−carbon, and (h) Pt nanoparticles of Pt/C.

In the normal pH range, the proton adsorption on SiOH surface groups is very low. Adding acid promotes the hydrolysis of TEOS and significantly increases the proton adsorption reaction of SiOH, leading to the formation of positively charged $SiOH_2^+$ and the rapid increase in the zeta potential.[24] In the presence of P123 chains, self-assembly between the silica with a surface proton and aether (C−O−C) sites in the PEO chain would be derived by hydrogen bonding (route 2 in Figure 1). The P123 polymer assembled on the silica surface stabilizes the silica nanoparticles and prevents grain growth. Thus, the tube-cumulated mesoporous phenolic oligomers/SiO_2 with the template of the P123 surfactant is formed through the hydrogen-bonding-assisted self-assembly between the phenolic oligomers/P123 triblock copolymer and $SiOH_2^+$/P123 triblock copolymer. With the phase separation of P123, the colloidal complex forms an ordered phenolic oligomers/SiO_2 framework. The template is then removed by heat treatment, with the SiO_2 nanoparticles anchored into the walls of the carbon mesoporous framework.

Figure 2 displays the TEM images of the meso-carbon and meso-SiO_2−carbon supports and the Pt electrocatalyst supported on meso-carbon, meso-SiO_2−carbon, and XC-72 carbon black. Ordered arrays of the mesoporous channels with a *d* spacing of ∼8 nm and a wall thickness of ∼3 nm are clearly displayed for both the meso-carbon and Pt−meso-carbon (Figure 2a,c). The mesoporous structure of the meso-SiO_2−carbon is very similar to that of the meso-carbon with highly ordered mesoporous channels (Figure 2b). This means that the ordered structure of mesoporous carbon is not disturbed by the incorporation of 5 wt % SiO_2. As shown in Figure 2c,d, the ordered arrays of both the meso-carbon and the meso-SiO_2−carbon supports are well maintained after the deposition of Pt nanoparticles. The enlarged images of the Pt electrocatalysts supported on meso-carbon, meso-SiO_2−carbon, and XC-72 clearly show the crystalline lattice of Pt nanoparticles (Figure 2f−h). For all of the supported Pt electrocatalysts studied here, Pt nanoparticles with an average particle size of 2 to 3 nm are uniformly dispersed on the surface of the carbon support.

Figure 3a shows the small-angle X-ray diffraction (SAXRD) spectra of Pt/meso-SiO_2−carbon, Pt/meso-carbon, and Pt/C electrocatalysts. As expected, Pt/C does not have diffraction peaks in the small-angle range, reflecting its disordered structure. The strong diffraction peak of Pt/meso-carbon and Pt/meso-SiO_2−carbon at a 2θ angle of ∼1° corresponds to the (100) lattice planes,[14,16] the existence of a mesoporous structure with long-range order, and 2D hexagonal symmetry similar to that of the carbon mesoporous material CMK-3.[25] The XRD peak intensity in Pt/meso-SiO_2−carbon slightly decreased compared to that of Pt/meso-carbon, which is possibly attributed to the interposition of silica nanoparticles into the mesoporous carbon phase, resulting in the reduced long-range order of the structure. The *d* spacing values of the (100) peaks of the Pt/meso-carbon and Pt/meso-SiO_2−carbon are 8.8 and 8.4 nm. The values are

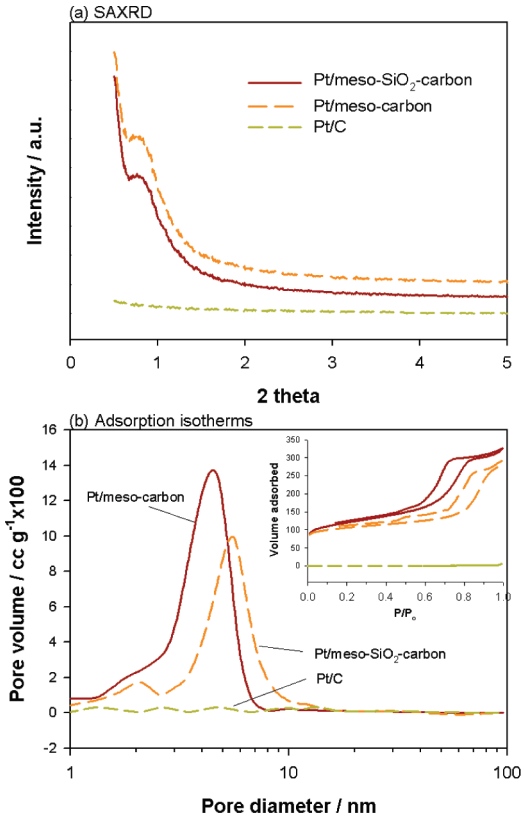

Figure 3. (a) Small-angle X-ray diffraction spectra and (b) pore size distribution of the Pt/meso-SiO_2−carbon, Pt/meso-carbon, and Pt/C electrocatalyst. The inserted graph in (b) is the corresponding N_2 adsorption−desorption isotherms of the samples.

obtained from Bragg's law, $d_{100} = \lambda/2 \sin \theta$, in which λ is the wavelength of the Cu Kα X-ray source (0.154 nm). Further calculation of the unit cell dimension of the mesoporous catalyst, α, were based on $a = 2d_{100}/\sqrt{3}$ (ref 26), and the results for the Pt/meso−carbon and Pt/meso-SiO_2−carbon are 10.2 and 9.7 nm, respectively.

Figure 3b shows the N_2 adsorption−desorption isotherms and the corresponding pore size distribution for the Pt/meso-SiO_2−carbon, Pt/meso-carbon, and Pt/C. The specific surface areas calculated from the adsorption isotherms are 416, 365, and 250 m^2/g for Pt/meso-carbon, Pt/meso-SiO_2−carbon, and Pt/C electrocatalysts, respectively. Very different from those of the Pt/C catalyst, the isotherms of the mesoporous samples are categorized into type IV and show large hysteresis loops. This feature is typical for mesoporous materials with narrow size distributions. The Pt/meso-carbon powders exhibit narrow pore size distributions with the main peak centered at 4.5 nm. A well-defined step in the adsorption and desorption curve of Pt/meso-carbon appears between relative partial pressures (P/P_o) of 0.65 and 0.75. The position of the sharp step in the isotherm shifts slightly to a relatively higher pressure for Pt/meso-SiO_2−carbon as compared to that for Pt/meso-carbon, indicating that there is a small increase in the mesopore size with the addition of silica. The diameter of the main pore for Pt/meso-SiO_2−carbon is ∼5.2 nm with a decrease in pore volume in this range and a small peak at 2 nm emerges that may be attributed to the introduction of silica nanostructure into the carbon arrays. On the basis of the unit cell dimension (a) from SAXRD and pore size from N_2 adsorption−desorption isotherms, the pore-wall thickness can be calculated because thickness = a − pore size.[27] The wall thicknesses for Pt/meso-carbon and Pt/meso-SiO_2−carbon are 5.7 and 4.5 nm, respectively, consistent with those evaluated from TEM images.

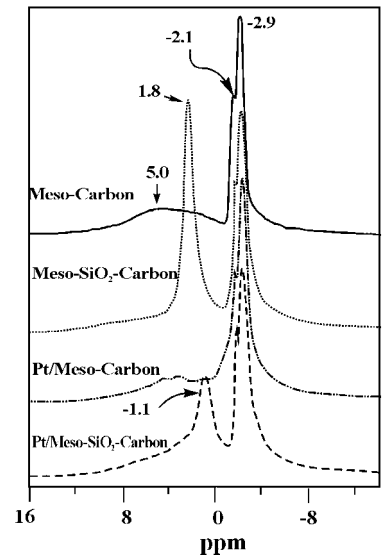

Figure 4. Solid-state ^1H spectra of meso-carbon, meso-SiO_2−carbon, Pt/meso-carbon, and Pt/meso-SiO_2−carbon.

The solid-state ^1H spectra of meso-carbon, meso-SiO_2−carbon, Pt/meso-carbon, and Pt/meso-SiO_2−carbon are displayed in Figure 4. The pure meso-carbon reveals three peaks in the ^1H spectrum: a weak, broad bump centered around 5 ppm that is assignable to the adsorbed water located out of carbon particles,[28,29] suggesting the difficulty of retaining water by bulk carbon; as a comparison, the most intense signal of the ^1H spectrum was located at $\delta_H \approx 2.9$ ppm with a shoulder peak at $\delta_H \approx 2.1$ ppm, which is assigned to the adsorbed water molecules in the narrow capillaries of the mesoporous structure.[28] Retaining water in the narrow channels of mesoporous structure through capillary condensation is reasonable because the saturated vapor pressure is much smaller in nanopores.[30] On the basis of the Kelvin and Young−Laplace equations,[11] the saturated vapor pressure decreases proportionally to the reduction in the capillary radius and would be reduced to about half the value with respect to that in the bulk when the radius is in the range of 3 to 5 nm. The high intensity of the capillary water is very important for the mesoporous carbon as a catalyst support for elevated-temperature PEMFCs because it could provide moisture/humidity to the Pt electrocatalysts located on the surface of meso-supports (outlet of the capillaries) by capillary force.[31]

After the incorporation of silica in the mesoporous carbon structure, a strong peak located at $\delta_H \approx 1.8$ ppm emerged, which is assigned to the hydrogen in the hydroxy groups (−OH) on the isolated silanol.[32] Hydrogen atoms could be related to hydroxyls and adsorbed water molecules on amorphous silica. The appearance of $\delta_H \approx 1.8$ ppm demonstrates the enhancement of the water-retention ability of the mesoporous carbon by the incorporated silica. The high intensity of the ^1H signal at $\delta_H \approx 1.8$ ppm indicates the much stronger water adsorption of silica as compared to that of carbon as a result of the high density of −OH on the silica particle surface. After the deposition of Pt nanoparticles, ^1H signals around 1.8 ppm are decreased for meso-SiO_2−carbon, coupled with shifting to a lower field, $\delta_H \approx 1.1$ ppm, reflecting the interaction of metal particles on the hydrogen bonds. The signals of water molecules in the mesopores at $\delta_H \approx 2.1-2.9$ ppm do not change after the Pt nanoparticle deposition, revealing that the Pt nanoparticles are deposited on the surface of the mesoporous structure.

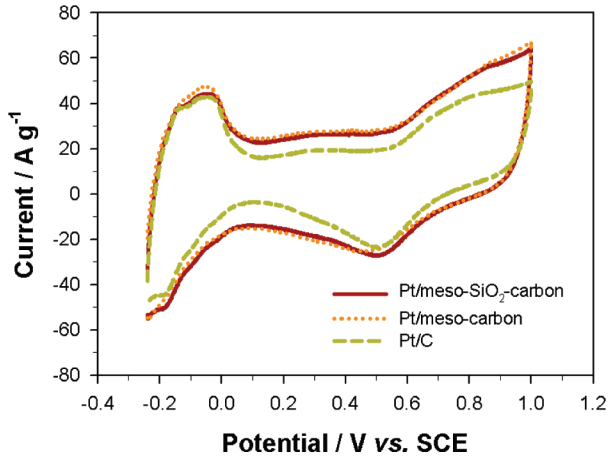

Figure 5. Cyclic voltammetric curves of Pt/meso-SiO_2−carbon, Pt/meso-carbon, and the Pt/C electrocatalyst measured in N_2-saturated 0.5 M H_2SO_4 at a scan rate of 10 mV/s.

3.2. Electrochemical Activity and Performance of Pt/meso-SiO_2−Carbon Electrocatalysts. The electrochemical properties of the Pt/meso-SiO_2−carbon, Pt/meso-carbon, and Pt/C electrocatalysts were characterized by cyclic voltammetry (CV) in a nitrogen-saturated 0.5 M H_2SO_4 solution (Figure 5). Pt/meso-SiO_2−carbon and Pt/meso-carbon electrocatalysts have similar cyclic voltammetry features, and the electrochemically active surface (EAS) can be calculated from the charge associated with the hydrogen reaction. The EAS values calculated for Pt/meso-carbon, Pt/meso-SiO_2−carbon, and Pt/XC-72 are 157, 151, and 144 m^2/g_{pt}, respectively. The similar EAS of the Pt electrocatalysts in this study is most likely due to the similar particle size of Pt nanoparticles on the three different types of carbon supports used in this work (Figure 2).

Figure 6 shows the polarization performance and impedance curves of single cells assembled with different Pt electrocatalysts under 100% relative humidity (RH) at 70 °C. The EIS spectra of the cells were recorded at a cell voltage of 0.9 V, close to the open circuit of ~0.94 V. The cells assembled with Pt/meso-carbon and Pt/meso-SiO_2−carbon electrocatalysts have a performance slightly higher than that of Pt/C electrocatalysts, particularly at high currents (Figure 6a). The maximum power density values for the cells with Pt/mso-SiO_2−carbon and Pt/meso-carbon electrocatalysts are 526 and 546 mW/cm^2, respectively, which are also higher than 491 mW/cm^2 for the cell with Pt/C electrocatalysts. This indicates the high water transport or discharging ability of the mesoporous structure.[33] The impedance responses are characterized by a single impedance arc over the whole frequency range, reflecting the charge-transfer dominance in the electrocatalyst layer (Figure 6b). The charge-transfer resistance, R_{ct}, values for the electrode reaction under 100% RH at 70 °C are 3.17 and 3.28 Ω for the cell with Pt/meso-SiO_2-carbon and Pt/meso-carbon electrocatalysts, respectively, which are slightly lower than 3.74 Ω for the cell with the conventional Pt/C electrocatalysts. The membrane resistance, R_m, of the cell is ~0.50 Ω for the cells with the Pt electrocatalysts with both mesoporous carbon and XC72 carbon. The similar values of R_{ct} and R_m indicate that the enhanced water retention properties of the meso-SiO_2−carbon and meso-carbon supports do not provide significant benefits to the electrochemical activity of the Pt electrocatalysts as compared to the conventional high surface carbon for PEMFCs operated under 100% RH. The polarization resistance, membrane resistance, and power densities of the cells are given in Table 1.

To demonstrate the water-retention properties of the Pt electrocatalyst supported on the meso-SiO_2−carbon, the fuel

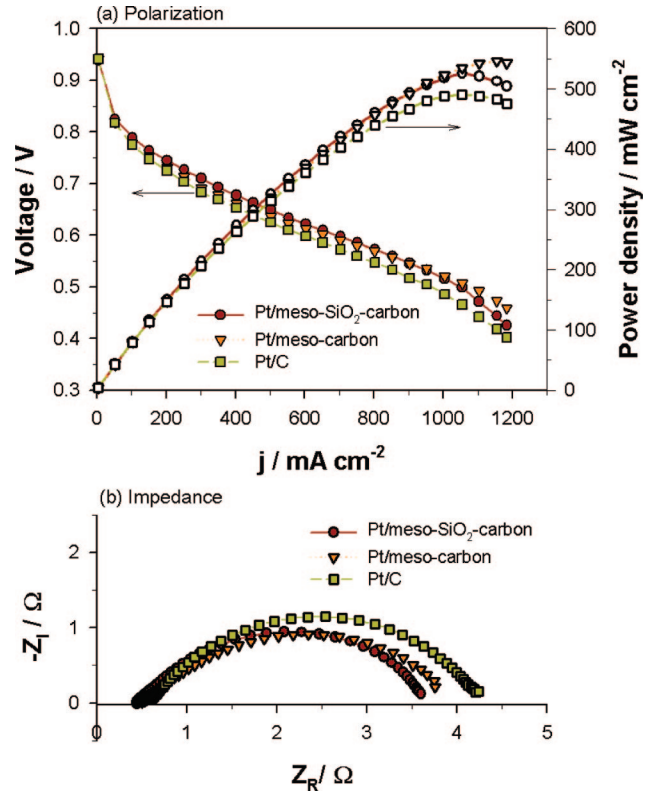

Figure 6. (a) Polarization performance and (b) impedance spectra of single cells assembled with Pt/meso-SiO_2−carbon, Pt/meso-carbon, and the Pt/C electrocatalyst. EIS curves were measured at a cell voltage of 0.9 V. Cell operating conditions: 70 °C, 100% RH under H_2/air; anode: Pt loading = 0.2 mg/cm^2; cathode: Pt loading = 0.4 mg/cm^2.

cells assembled with various Pt electrocatalysts were tested at 100 °C and a reduced RH of 30%, as shown in Figure 7a. The performance of the cell assembled with conventional Pt/C electrocatalysts decreases sharply in the low current density region, suggesting the rapid dehydration of the cell at elevated high temperatures and low humidity conditions. The performance then recovers slightly with the increasing of current most likely because of the water produced in the cell. For the cells assembled with Pt/meso-SiO_2−carbon and Pt/meso-carbon electrocatalysts, the initial voltage drop is much slower, indicating the significantly better water retention abilities of the mesoporous supports. The maximum power density is 456 mW/cm^2 for the cell with Pt/meso-SiO_2−carbon and higher than 417 mW/cm^2 for the cell with Pt/meso-carbon electrocatalysts. The better power output for the cell with the Pt/meso-SiO_2−carbon electrocatalysts as compared to that with Pt/meso-carbon is clearly due to the improved water retention properties of the incorporated silica in the mesorous carbon structure. The power density for the cell with conventional Pt/C electrocatalysts is 345 mW/cm^2, which is significantly lower than for the cells with mesoporous supports. The results show that the mesoporous supports are most beneficial for the PEMFCs operated at elevated high temperature and reduced humidity conditions.

The high performance of the cells with the Pt/meso-SiO_2−carbon and Pt/meso-carbon electrocatalysts is also supported by the impedance responses of the cells measured at a cell voltage of 0.85 V, as shown in Figure 7b. The impedance responses are characterized by a single arc, similar to that of the cells operated at 70 °C and 100% RH. However, the size of the impedance arc for the reaction on the cells with Pt/meso-SiO_2−carbon and Pt/meso-carbon is significantly smaller than that of the cell with Pt/C. R_{ct} values for the cells assembled

TABLE 1: Properties and Performance of Pt Electrocatalysts and Cells Assembled with Different Pt Electrocatalysts Operated Under Different Conditions

	EAS	at 70°C, 100%RH			at 100°C, 30%RH		
electrocatalyst	m^2/g_{Pt}	R_m/Ω	R_{ct}/Ω	$P_{max}/mW/cm^2$	R_m/Ω	R_{ct}/Ω	$P_{max}/mW/cm^2$
Pt/meso-SiO_2-carbon	151	0.50	3.17	526	0.83	1.34	456
Pt/meso-carbon	157	0.49	3.28	546	0.91	1.98	417
Pt/C	144	0.52	3.74	491	1.07	3.96	345

with the Pt/meso-carbon and Pt/meso-SiO_2−carbon electrocatalysts are 1.98 and 1.34 Ω, which are much smaller than 3.96 Ω for the cell assembled with conventional Pt/C electrocatalysts. Also, the R_m for the cell assembled with the Pt/meso-SiO_2−carbon and Pt/meso-carbon is 0.83−0.91 Ω, which is significantly lower than 1.07 Ω measured on the cell assembled with the Pt/C electrocatalysts. The lower membrane resistance of the cells based on the Pt/meso-carbon and Pt/meso-SiO_2−carbon electrocatalysts is most likely related to the high water-retention abilities of the meso-carbon and meso-SiO_2−carbon supports in the catalyst layer to supply water to humidify the membrane under a reduced RH of 30%. Under operating conditions of 100 °C and 30% RH, the best performance was observed for the cell assembled with Pt/meso-SiO_2−carbon with the lowest R_{ct} and R_m and the highest power density. This demonstrates that the incorporation of hydrophilic silica into the mesoporous carbon enhances the self-humidifying properties of mesoporous carbon supports in PEMFCs. Nevertheless, the cell performance at 100 °C and 30% RH is lower than for the cell operated at 70 °C and 100% RH. The reduced cell performance at elevated temperature and reduced humidity is likely due to the dehydration of the Nafion membrane, which leads to the increase in the cell membrane resistance, R_m (Table 1).

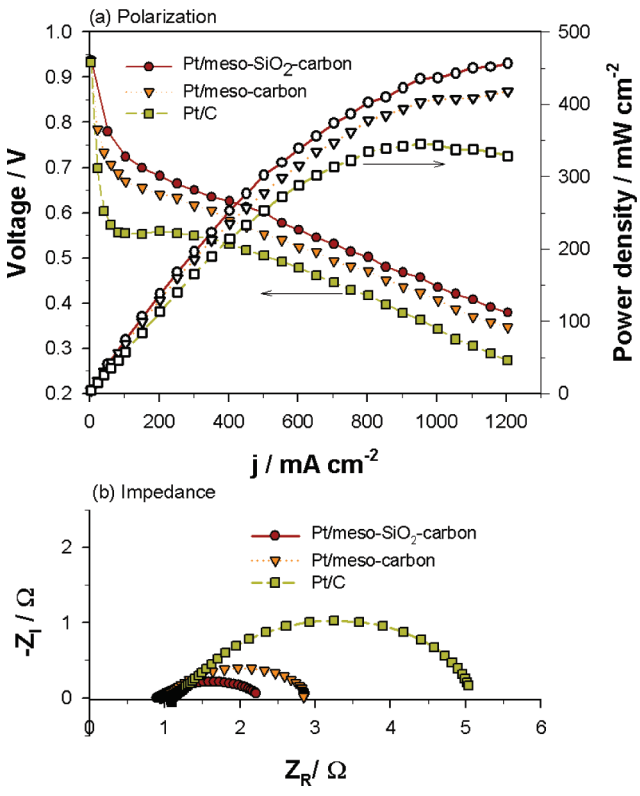

Figure 7. (a) Polarization performance and (b) impedance spectra of single cells assembled with Pt/meso-SiO_2−carbon, Pt/meso-carbon, and Pt/C electrocatalyst. EIS curves were measured at a cell voltage of 0.85 V. Cell operating conditions: 100 °C, 30% RH under H_2/air; anode: Pt loading = 0.2 mg/cm^2; cathode: Pt loading = 0.4 mg/cm^2.

The reason for the performance drop of the cell operated at elevated temperatures and reduced RH is the dehydration in the electrocatalyst layer and the electrolyte membrane, leading to reduced proton conductivity and the increase in the membrane resistance. The reduced humidity also increases the charge-transfer resistance of the electrode reaction occurring at the catalyst layer and electrolyte membrane interface regions because of the restricted proton transferring to the active site in the catalyst layer. In the situation of mesoporous carbon, the mesopores are highly ordered. As the saturated vapor pressure p_w^{vap} decreases with the pore size, water condensation would occur in the pores if the water vapor pressure is higher than the saturated vapor pressure inside the pore. The value of p_w^{vap} can be calculated according to[3,34]

$$p_w^{vap} = p_{w,o}^{vap} \exp\left(\frac{-2aV_w r \cos\theta}{dRT}\right) \quad (1)$$

where $p_{w,o}^{vap}$ is the normal vapor pressure of water, r is the surface tension of water (6.58×10^{-2} N/m for 70 °C and 6.168×10^{-2} N/m for 100 °C, respectively), R is the ideal gas constant, T is the absolute temperature, V_w is the molar volume of water, θ is the contact angle between water and the pore surface (81° for mesoporous carbon and 68° for silica-coated mesoporous carbon, as measured by the Kyowa contact angle meter[35]), d is the diameter of the pore, and a is the constant for the cylinder mesopores (which is 2). Hence, the ratio of the water vapor pressure for water condensation in the mesoporous pores to the normal water pressure, $p_w^{vap}/p_{w,o}^{vap}$ could be estimated under the PEMFCs operating conditions:

$$p_w^{vap}/p_{w,o}^{vap} = \exp\left(-\frac{2aV_w r}{R}\frac{\cos\theta}{dT}\right) \quad (2)$$

For the meso-carbon and meso-SiO_2−carbon with the size of mesopores in the range of 4.5−5.2 nm, the $p_w^{vap}/p_{w,o}^{vap}$ ratio is calculated to be ~0.3 and 0.6 at 100 °C, respectively. This indicates that under normal operating conditions at elevated temperature and reduced RH, the water vapor pressure supplied by the external humidity and the water produced from the H_2/O_2 reaction would be higher than the $p_w^{vap}/p_{w,o}^{vap}$ value, resulting in the condensation and adsorption of water in the mesoporous capillaries. The condensed water could be released if the water vapor pressure is depleted in the electrocatalyst layer, providing moisture and humidity to the electrocatalyst and membrane interface. However, for the conventional high surface area carbon black XC-72, the pore size is about 0.05−1 μm,[33] and the corresponding $p_w^{vap}/p_{w,o}^{vap}$ ratio is in the range of 0.95−1, which is very close to unity. This indicates that water condensation could occur only in high surface area carbon under 100% RH. Thus, the water retention ability of conventional high surface area carbon is poor. This explains the significant performance drop of the cell assembled with Pt/C electrocatalysts under operating conditions of 100 °C and 30% RH (Figure 7a). The differences in the $p_w^{vap}/p_{w,o}^{vap}$ ratios for the mesoporous silica−carbon and conventional carbon demonstrate the advantages of meso-

porous materials as Pt electrocatalysts supports for PEMFCs operated at elevated temperature and reduced humidity conditions.

4. Conclusions

Highly ordered meso-carbon and meso-SiO_2−carbon electrocatalyst supports were synthesized and characterized for PEM fuel cells operated under elevated temperature and reduced RH conditions. Hydrophilic silica was incorporated into the mesoporous carbon nanostructure through a hydrogen-bonding-assisted self-assembly route. The pore diameters of the Pt/meso-carbon and Pt/meso-SiO_2−carbon catalyst are 4.5 and 5.2 nm, respectively, and the solid-state ^1H spectrum demonstrates the water condensation inside the capillaries of the mesoporous structure and the enhanced water retention in the mesoporous supports by the incorporation of hydrophilic silica. Pt/meso-carbon and Pt/meso-SiO_2−carbon electrocatalysts perform better than the cell assembled with conventional Pt/C electrocatalysts, particularly for the PEMFCs operated under elevated temperature and reduced humidity conditions. The use of meso-carbon and meso-SiO_2−carbon materials as electrocatalyst supports is beneficial to enhancing the self-humidifying ability of the electrocatalyst layer, thus improving the cell performance at elevated high temperature and relatively low humidity.

References and Notes

(1) Stumper, J.; Stone, C. *J. Power Sources* **2008**, *176*, 468. Wei, Z. D.; Yan, C.; Tan, Y.; Li, L.; Sun, C. X.; Shao, Z. G.; Shen, P. K.; Dong, H. W. *J. Phys. Chem. C* **2008**, *112*, 2671. Agnolucci, P. *Int. J. Hydrogen Energy* **2007**, *32*, 4306. Agnolucci, P. *Int. J. Hydrogen Energy* **2007**, *32*, 3526. DOE 2006 Annual Progress Report: DOE Hydrogen Program, Department of Energy, 2007.

(2) Li, Q. F.; He, R. H.; Jensen, J. O.; Bjerrum, N. J. *Chem. Mater.* **2003**, *15*, 4896. Zhang, J. L.; Xie, Z.; Zhang, J. J.; Tanga, Y. H.; Song, C. J.; Navessin, T.; Shi, Z. Q.; Song, D. T.; Wang, H. J.; Wilkinson, D. P.; Liu, Z. S.; Holdcroft, S. *J. Power Sources* **2006**, *160*, 872.

(3) Park, M. J.; Downing, K. H.; Jackson, A.; Gomez, E. D.; Minor, A. M.; Cookson, D.; Weber, A. Z.; Balsara, N. P. *Nano Lett.* **2007**, *7*, 3547.

(4) Damjanvic, A. In *Modern Aspects of Electrochemistry*; 1969; Vol. 5.

(5) Shao, Y. Y.; Yin, G. P.; Wang, Z. B.; Gao, Y. Z. *J. Power Sources* **2007**, *167*, 235.

(6) Tang, H.; Wan, Z.; Pan, M.; Jiang, S. P. *Electrochem. Commun.* **2007**, *9*, 2003. Zhu, J.; Tang, H. L.; Pan, M. *J. Membr. Sci.* **2008**, *312*, 41. Zhu, X. B.; Zhang, H. M.; Liang, Y. M.; Zhang, Y.; Luo, Q. T.; Bi, C.; Yi, B. L. *J. Mater. Chem.* **2007**, *17*, 386. Zhu, X. B.; Zhang, H. M.; Zhang, Y.; Liang, Y. M.; Wang, X. L.; Yi, B. L. *J. Phys. Chem. B* **2006**, *110*, 14240. Zhang, W. J.; Li, M. K. S.; Yue, P. L.; Gao, P. *Langmuir* **2008**, *24*, 2663. Sanchez, C.; Julian, B.; Belleville, P.; Popall, M. *J. Mater. Chem.* **2005**, *15*, 3559. Binsu, V. V.; Nagarale, R. K.; Shahi, V. K. *J. Mater. Chem.* **2005**, *15*, 4823. Pereira, F.; Valle, K.; Belleville, P.; Morin, A.; Lambert, S.; Sanchez, C. *Chem. Mater.* **2008**, *20*, 1710. Hao, H. S.; Cui, J. H.; Chen, C. Q.; Pan, L. J.; Hu, J.; Hu, X. *Solid State Ionics* **2006**, *177*, 631. Athens, G. L.; Ein-Eli, Y.; Chmelka, B. F. *Adv. Mater.* **2007**, *19*, 2580.

(7) Han, M.; Chan, S. H.; Jiang, S. P. *Int. J. Hydrogen Energy* **2007**, *32*, 385. Kim, J. H.; Kim, H. J.; Lim, T. H.; Lee, H. I. *J. Power Sources* **2007**, *170*, 275. Jung, U. H.; Park, K. T.; Park, E. H.; Kim, S. H. *J. Power Sources* **2006**, *159*, 529. Sahu, A. K.; Selvarani, G.; Pitchumani, S.; Sridhar, P.; Shukla, A. K. *J. Appl. Electrochem.* **2007**, *37*, 913.

(8) Vengatesan, S.; Kim, H. J.; Lee, S. Y.; Cho, E.; Ha, H. Y.; Oh, I. H.; Hong, S. A.; Lim, T. H. *Int. J. Hydrogen Energy* **2008**, *33*, 171.

(9) Kannan, A. M.; Cindrella, L.; Munukutla, L. *Electrochim. Acta* **2008**, *53*, 2416.

(10) Aharoni, C. *Langmuir* **1997**, *13*, 1270. Grosman, A.; Ortega, C. *Langmuir* **2005**, *21*, 10515. Kohonen, M. M.; Christenson, H. K. *Langmuir* **2000**, *16*, 7285. Bocquet, L.; Charlaix, E.; Ciliberto, S.; Crassous, J. *Nature* **1998**, *396*, 735.

(11) Dullien, F. A. L. *Transp. Porous Media* **1991**, *6*, 581.

(12) Chang, H.; Joo, S. H.; Pak, C. *J. Mater. Chem.y* **2007**, *17*, 3078. Liu, S. H.; Yu, W. Y.; Chen, C. H.; Lo, A. Y.; Hwang, B. J.; Chien, S. H.; Liu, S. B. *Chem. Mater.* **2008**, *20*, 1622. Ng, Y. H.; Ikeda, S.; Harada, T.; Park, S.; Sakata, T.; Mori, H.; Matsumura, M. *Chem. Mater.* **2008**, *20*, 1154.

(13) Joo, S. H.; Choi, S. J.; Oh, I.; Kwak, J.; Liu, Z.; Terasaki, O.; Ryoo, R. *Nature* **2001**, *412*, 169.

(14) Liu, S. H.; Lu, R. F.; Huang, S. J.; Lo, A. Y.; Chien, S. H.; Liu, S. B. *Chem. Commun.* **2006**, 3435.

(15) Su, F. B.; Zeng, J. H.; Bao, X. Y.; Yu, Y. S.; Lee, J. Y.; Zhao, X. S. *Chem. Mater.* **2005**, *17*, 3960. Ding, J.; Chan, K. Y.; Ren, J. W.; Xiao, F. S. *Electrochim. Acta* **2005**, *50*, 3131. Joo, J. B.; Kim, P.; Kim, W.; Kim, J.; Yi, J. *Catal. Today* **2006**, *111*, 171. Wen, Z. H.; Liu, J.; Li, J. H. *Adv. Mater.* **2008**, *20*, 743. Zhou, J. H.; He, J. P.; Zhao, G. W.; Zhang, C. X.; Wang, T.; Chen, X. *Electrochem. Commun.* **2008**, *10*, 76.

(16) Lei, Z. B.; Bai, S. Y.; Xiao, Y.; Dang, L. Q.; An, L. Z.; Zhang, G. N.; Xu, Q. *J. Phys. Chem. C* **2008**, *112*, 722.

(17) Lin, M. L.; Huang, C. C.; Lo, M. Y.; Mou, C. Y. *J. Phys. Chem. C* **2008**, *112*, 867.

(18) Liang, C. D.; Dai, S. *J. Am. Chem. Soc.* **2006**, *128*, 5316.

(19) Meng, H.; Shen, P. K. *J. Phys. Chem. B* **2005**, *109*, 22705.

(20) Tang, H. L.; Wang, S. L.; Jiang, S. P.; Pan, M. *J. Power Sources* **2007**, *170*, 140.

(21) Rodriguez, A. T.; Li, X. F.; Wang, J.; Steen, W. A.; Fan, H. Y. *Adv. Funct. Mater.* **2007**, *17*, 2710.

(22) Tang, H.; Wan, Z.; Pan, M.; Jiang, S. P. *Electrochem. Commun.* **2007**, *9*, 2003.

(23) Hiemstra, T.; Vanriemsdijk, W. H.; Bolt, G. H. *J. Colloid Interface Sci.* **1989**, *133*, 91. Hiemstra, T.; Dewit, J. C. M.; Vanriemsdijk, W. H. *J. Colloid Interface Sci.* **1989**, *133*, 105.

(24) Pettersson, A.; Rosenholm, J. B. *Langmuir* **2002**, *18*, 8447.

(25) Zhou, H. S.; Zhu, S. M.; Hibino, M.; Honma, I.; Ichihara, M. *Adv. Mater.* **2003**, *15*, 2107. Lu, A. H.; Schmidt, W.; Taguchi, A.; Spliethoff, B.; Tesche, B.; Schuth, F. *Angew. Chem., Int. Ed.* **2002**, *41*, 3489. Roggenbuck, J.; Tiemann, M. *J. Am. Chem. Soc.* **2005**, *127*, 1096. Wang, Y. G.; Cheng, L.; Li, F.; Xiong, H. M.; Xia, Y. Y. *Chem. Mater.* **2007**, *19*, 2095.

(26) Xia, Y. D.; Mokaya, R. *Adv. Mater.* **2004**, *16*, 886.

(27) Gao, P.; Wang, A.; Wang, X.; Zhang, T. *Chem. Mater.* **2008**, *20*, 1881.

(28) Gun'ko, V. M.; Kozynchenko, O. P.; Turov, V. V.; Tennison, S. R.; Zarko, V. I.; Nychiporuk, Y. M.; Kulik, T. V.; Palyanytsya, B. B.; Osovskii, V. D.; Ptushinskii, Y.; Turov, A. V. *Colloids Surf., A* **2008**, *317*, 377.

(29) Kim, H. J.; Shul, Y. G.; Han, H. *Appl. Catal. A* **2006**, *299*, 46. Rao, P. M.; Goldberg-Oppenheimer, P.; Kababya, S.; Vega, S.; Landau, M. *J. Mol. Catal. A* **2007**, *275*, 214. Liu, C. H. C.; Maciel, G. E. *J. Am. Chem. Soc.* **1996**, *118*, 5103.

(30) Kityk, A. V.; Hofmann, T.; Knorr, K. Phys. Rev. Lett. 2008, *1*;Rojas, F.; Kornhauser, I.; Felipe, C.; Esparza, J. M.; Cordero, S.; Dominguez, A.; Riccardo, J. L. *Phys. Chem. Chem. Phys.* **2002**, *4*, 2346. Machin, W. D. *Phys. Chem. Chem. Phys.* **2003**, *5*, 203. Floquet, N.; Coulomb, J. P.; Dufau, N.; Andre, G.; Kahn, R. *Adsorption* **2005**, *11*, 139. Dourdain, S.; Gibaud, A. Appl. Phys. Lett. 2005, *87*. Detcheverry, F.; Kierlik, E.; Rosinberg, M. L.; Tarjus, G. *Adsorption* **2005**, *11*, 115. Armatas, G. S.; Salmas, C. E.; Louloudi, M.; Androutsopoulos, G. P.; Pomonis, P. J. *Langmuir* **2003**, *19*, 3128.

(31) Huber, P.; Gruner, S.; Schafer, C.; Knorr, K.; Kityk, A. V. *Eur. Phys. J.* **2007**, *141*, 101.

(32) Doremieux Morin, C.; Heeribout, L.; Dumousseaux, C.; Fraissard, J.; Hommel, H.; Legrand, A. P. *J. Am. Chem. Soc.* **1996**, *118*, 13040. Bronnimann, C. E.; Zeigler, R. C.; Maciel, G. E. *J. Am. Chem. Soc.* **1988**, *110*, 2023.

(33) Tang, H. L.; Wang, S. L.; Pan, M.; Yuan, R. Z. *J. Power Sources* **2007**, *166*, 41.

(34) Dullien, F. A. L. *Transp. Porous Media* **1991**, *6*, 581.

(35) Zhu, J.; Tang, H. L.; Pan, M. *J. Membr. Sci.* **2008**, *312*, 41.

JP8066662